Spatial and seasonal variations of stable isotope ratios of particulate organic carbon and nitrogen in the surface water of the Kuroshio

Taketoshi Kodama[1], Atsushi Nishimoto[2], Sachiko Horii[3], Daiki Ito[4], Tamaha Yamaguchi[4], Kiyotaka Hidaka[1], Takashi Setou[5], and Tsuneo Ono[6]

[1]Fisheries Resources Institute, Japan Fisheries Research and Education Agency
[2]Fisheries Technology Institute, Japan Fisheries Research and Education Agency
[3]Seikai National Fisheries Research Institute
[4]National Research Institute of Fisheries Science
[5]Fisheries Research Agency
[6]National Research Institute for Fisheries Science / Fisheries Research Agency

November 22, 2022

Abstract

Stable isotope ratios of carbon and nitrogen (δ^{13}C and δ^{15}N) in the particulate organic matter (POM) of the euphotic layer were seasonally investigated in the vicinity of the Kuroshio from 2008 to 2019 (n = 490). Generalized linear models (GLMs) showed significant seasonality of δ^{13}C and δ^{15}N of POM in the coastal (between Japan Main Island and the northern edge of the Kuroshio) and offshore (Kuroshio and more southern parts) areas. Seasonal climatological δ^{13}C estimated based on the GLMs and seasonal median values of the environmental parameters was the highest in summer (-22.4 $\pm$ 0.2-22.9 +- 0.2in winter in both areas (-23.9 +- 0.2and offshore areas, respectively). Seasonal climatological δ^{15}N showed different spatial variations from spring to summer. The δ^{15}N value was the lowest during winter (0.8 $\pm$ 0.4seasons in the coastal area (~3nitrate originating in the deep-sea water was the main source of new production from spring to autumn. In contrast, δ15N in the offshore areas decreased from spring (2.6 $\pm$ 0.4suggesting that the significant contributions of atmospheric deposition and nitrogen fixation in the summer were similar to those around Hawaii. Therefore, the nitrogen sources for biological production were different between the areas and seasons in the vicinity of the Kuroshio.

1 **Spatial and seasonal variations of stable isotope ratios of particulate organic carbon**

2 **and nitrogen in the surface water of the Kuroshio**

3

4 **KODAMA Taketoshi[1,*]; NISHIMOTO Atsushi[2]; HORII Sachiko[3]; ITO Daiki[1];**

5 **YAMAGUCHI Tamaha[1]; HIDAKA Kiyotaka[1]; SETOU Takashi[1]; ONO Tsuneo[1]**

6 [1]Fisheries Resources Institute, Japan Fisheries Research and Education Agency

7 [2]Fisheries Technology Institute, Japan Fisheries Research and Education Agency

8 [3]Nagasaki Field Station, Fisheries Resources Institute, Japan Fisheries Research and Education

9 Agency

10 *Corresponding author

11 Address: 2-12-4 Fukuura, Kanazawa, Yokohama, Kanagawa 236-8648, Japan

12 e-mail: takekodama@affrc.go.jp

13

14 Running title: Stable isotope ratios of POM in the Kuroshio

15

16 **Key Points:**

17 • Stable isotope ratios of carbon and nitrogen in particulate organic matter (POM) are

18 seasonally investigated in the vicinity of the Kuroshio

19 • Generalized linear models show significant seasonality of $\delta^{13}C$ and $\delta^{15}N$ in the POM in

20 coastal and offshore areas

21 • Atmospheric deposition and nitrogen fixation are contributed to primary production in

22 the summer of the offshore area

23

24   **Abstract**

25   Stable isotope ratios of carbon and nitrogen (δ^{13}C and δ^{15}N) in the particulate organic matter

26   (POM) of the euphotic layer were seasonally investigated in the vicinity of the Kuroshio from

27   2008 to 2019 ($n = 490$). Generalized linear models (GLMs) showed significant seasonality of

28   δ^{13}C and δ^{15}N of POM in the coastal (between Japan Main Island and the northern edge of the

29   Kuroshio) and offshore (Kuroshio and more southern parts) areas. Seasonal climatological δ^{13}C

30   estimated based on the GLMs and seasonal median values of the environmental parameters was

31   the highest in summer (-22.4 ± 0.2‰ and -22.9 ± 0.2‰ in the coastal and offshore areas,

32   respectively) and lowest in winter in both areas (-23.9 ± 0.2‰ and -24.3 ± 0.2‰ in the coastal

33   and offshore areas, respectively). Seasonal climatological δ^{15}N showed different spatial

34   variations from spring to summer. The δ^{15}N value was the lowest during winter (0.8 ± 0.4‰),

35   and increased to a similar level during the other three seasons in the coastal area (~3‰),

36   suggesting that nitrate originating in the deep-sea water was the main source of new production

37   from spring to autumn. In contrast, δ^{15}N in the offshore areas decreased from spring (2.6 ±

38   0.4‰) to summer (0.9 ± 0.4‰), suggesting that the significant contributions of atmospheric

39   deposition and nitrogen fixation in the summer were similar to those around Hawaii.   Therefore,

40   the nitrogen sources for biological production were different between the areas and seasons in

41   the vicinity of the Kuroshio.

42

43   Keywords: Particulate organic matter, Kuroshio, δ^{13}C, δ^{15}N, N_2 fixation, diatoms

44

1. Introduction

The ocean absorbs large amounts of carbon and nitrogen, which have continuously increased after the industrial revolution [*Archer et al.*, 2009; *Duce et al.*, 2008; *Fowler et al.*, 2013]. To detect the variations of the carbon and nitrogen dynamics in the ocean, the stable isotope ratios of carbon and nitrogen are useful tracers [*Gruber et al.*, 1999; *Keeling*, 1979; *Sigman et al.*, 2009; *Sonnerup et al.*, 1999]. The proportion of ^{13}C to ^{12}C in soluble carbon dioxide in seawater has linearly decreased at a rate of 0.2–0.1‰ decade^{-1} with an increase in the carbon dioxide concentration in the atmosphere [*Gruber et al.*, 1999; *Sonnerup et al.*, 1999]. The long-term linear changes in the ratio of ^{15}N to ^{14}N have been rarely detected in the previous studies of the ocean [*Chiba et al.*, 2012; *Christensen and Richardson*, 2008], but the ratio of ^{15}N to ^{14}N in the coral skeleton-bound organic matter is decreasing with an increase in the anthropogenic nitrogen deposition in this century [*Ren et al.*, 2017].

The Kuroshio is the western boundary current of the North Pacific, and affects the long-term anthropogenic changes in the nitrogen and carbon dynamics [*Ishii et al.*, 2011; *Watanabe et al.*, 2005]. The dynamic also varies seasonally with the physical processes [*Kodama et al.*, 2014b]; the deep convection occurs in winter, while strong stratification occurs in summer. With strong stratification and increase in the surface water temperature, there is an abundance of dinitrogen-fixation cyanobacteria and bacteria in the summer [*Shiozaki et al.*, 2018; *Shiozaki et al.*, 2015]. In addition, water is horizontally transported from the marginal seas and/or the coastal areas to the Kuroshio [*Kodama et al.*, 2015; *Shiozaki et al.*, 2015]. These complex carbon and nitrogen dynamics may support and affect biological productivity in the Kuroshio. The low trophic production in the Kuroshio is one of the most important keys of the fishery resources in Japan and the Pan-Pacific countries. The Kuroshio area is the spawning and nursery

68 ground for many types of small pelagic fishes, *e.g.* sardine (*Sardinops melanostictus*), and

69 anchovy (*Engraulis japonicus*), in spring [*Ohshimo et al.*, 2019], and migratory tunas, *e.g.*

70 pacific bluefin tuna (*Thunnus orientalis*), yellowfin tuna (*T. albacares*), and skipjack tuna

71 (*Katsuwonus pelamis*), in the summer [*Tanaka et al.*, 2019; *Tawa et al.*, 2020].

72   The knowledge of the primary production processes in the vicinity of the Kuroshio is

73 limited. In general, determination of the stable isotope ratios of the phytoplankton can be

74 beneficial in understanding the primary production processes. For example, *Mino et al.* [2020]

75 investigated the seasonal variations in the stable isotope ratios of the settling particulate organic

76 matter (POM) collected outside the Kuroshio (station S1: 30°N, 145°E) with sediment traps and

77 reported that the nitrate supplied by deep-sea water accounted for ~90% of the annual new

78 production in this area and the remnant corresponded to the biological nitrogen fixation. A

79 mixture of living and nonliving organic matter exists in the real ocean and it is difficult to

80 separate these [*Volkman and Tanoue*, 2002]; therefore POM, occasionally named seston, is

81 conventionally treated as the proxy of phytoplankton. Stable isotope ratios of the POM are also

82 useful in understanding the grazing food chain, and subsequently the marine ecosystem. The

83 nitrogen isotope ratio of the POM is typically reflected in that of the large predators [*Aita et al.*,

84 2011; *Horii et al.*, 2018]. *Ohshimo et al.* [2019] determined the carbon and nitrogen isotope

85 ratios in the muscle of the pelagic forage fish and squid in the western North Pacific and reported

86 that their nitrogen isoscape possibly reflected the balance of nitrogen fixation and denitrification,

87 but did not investigate the stable isotope ratios of the POM. In the vicinity of the Kuroshio, fifty-

88 year repeat observations were conducted along 137°E [*Oka et al.*, 2018], but the stable isotope

89 ratios of the marine organisms including those of the POM were not measured in these

90 observations.

91　　　*Ohshimo et al.* [2019] determined both the high and low nitrogen isotope ratios in pelagic

92　　forage fish and squid found in the Kuroshio area, and reported that detailed analysis of the stable

93　　isotope ratios of the POM were necessary for understanding the grazing food chain and marine

94　　ecosystem of this area.　Therefore, in this study, carbon and nitrogen stable isotope ratios of the

95　　POM in the area adjacent to the Kuroshio water are determined in the over decadal seasonal

96　　investigations.　The seasonal and yearly variations in the stable isotope ratios of the POM are

97　　examined using environmental factors and empirical models, followed by the evaluation of the

98　　seasonal climatological values of the stable isotope ratios.　The goal of this study is to provide

99　　insights into the carbon and nitrogen dynamics in the Kuroshio area, in particular, the nitrogen

100　source for the primary production in this area.

101

102　2.　Materials and methods

103　2.1.　Observation

104　　　POM and environmental data were collected from 2008 to 2019 along the 138°E

105　coordinate between 34°30'N and 27°N (named as "O-line") [*Figure 1*] using R/V *Soyo-maru* of

106　Japan Fisheries Research and Education Agency.　The Kuroshio usually flows 32–33°N at

107　138°E; however, after the Kuroshio large meander in 2017, it flows between 30–32°N [*Figure*

108　*1*].　As the Kuroshio shows spatial contrast in the biogeochemical conditions between its

109　northern and southern parts [*Kodama et al.*, 2014b], the observation areas were divided as the

110　coastal (>13 nautical miles north to the Kuroshio axis) and offshore (the Kuroshio and southern

111　part of the Kuroshio axis) areas.　The position of the Kuroshio axis was defined as the monthly

112　mean values of the position in the Quick Bulletin of Ocean Conditions published by the Japan

113　Coast Guard (www1.kaiho.mlit.go.jp/KANKYO/KAIYO/qboc/index_E.html).

114   The POM sampling was conducted seasonally from 2008 to 2015, and the observations

115   were limited to the summer (August or September) and winter (January or February) after 2016

116   *[Figure 1]*. In summary, the observations were conducted at 23 stations in winter, 30 stations in

117   spring (March, April, or May), 28 stations in summer, and 21 stations in autumn (October or

118   November). After measuring the vertical distributions of the photosensitive available radiation

119   (PAR) using a discreate PAR sensor (PRR-800 or INF-300, Biospherical Instruments Inc., San

120   Diego, California, USA), the water samples were collected using the 12-L X-Niskin bottles

121   attached directly to the cable at five different water depths for which the PAR values were 100,

122   50, 25, 10, and 1% relative to the surface until May 2016. The sampling depth was fixed after

123   May 2016 within the upper 50 m. The vertical profiles of temperature and salinity were

124   measured using a conductivity-temperature-depth (CTD) sensor (SBE9plus, Sea-Bird Scientific,

125   Washington, USA). The discrete samples for determining nutrient and chlorophyll *a*

126   concentrations were obtained using the Niskin bottles attached to the CTD-CMS (Carousel

127   Multisampling System). Vertical resolution of the discrete samples (nutrients and chlorophyll *a*

128   concentrations) was 10 m depth. As the environmental parameters determined using the POM

129   samples were limited, the nearest depth data collected by the CTD-CMS was adopted for the

130   following statistical analysis. The details of the nutrient and chlorophyll *a* analyses were

131   previously reported in the literature [*Kodama et al.*, 2014b]. To treat the common-logarithm

132   transformed values, the nitrate concentration below 0.01 µM was set as 0.01 µM.

133   Diatom abundance was investigated at a depth of 10 m for some stations. One liter of

134   seawater samples were collected and fixed with glutaraldehyde solution. The carbon amount of

135   the diatom cells was calculated based on the lengths of the major axes and shapes [*Menden-*

136   *Deuer and Lessard*, 2000]. The number of one of the major dinitrogen fixation cyanobacteria,

137   *Trichodesmium,* was also counted. These were sporadically present regardless of the season and

138   mostly negligible; therefore, these results are not included.

139

140   **2.2.   Isotope analysis**

141   To measure the carbon and nitrogen stable isotope ratios of the POM, three liter of

142   seawater samples were filtered using a pre-combusted (450 °C, 6 h) glass fiber filter (Whatman

143   GF/F, Whatman). The amount of seawater was < 3 L in some case when the filtration time was

144   long. After filtration on board, the samples were kept frozen (-30 °C). In the on-land laboratory,

145   the samples were dried in a dry oven (60 °C, overnight) and kept in a desiccator until

146   decarboxylation.

147   Before measuring the isotope ratio, the samples were exposed to HCl fumes for more

148   than two hours to remove the carbonate salt. After drying again in the dry oven, the colored

149   surfaces of the glass filters were scraped off, and their stable isotope ratios were measured using

150   an isotopic ratio mass spectrometer (MAT 252, Thermo Fisher Scientific (Waltham,

151   Massachusetts, USA) till October 2013, and thereafter, using Isoprime 100 (Elementar,

152   Langenselbold, Germany). The stable isotope ratios of carbon and nitrogen were calibrated

153   using the curves obtained with L-alanine during the measurements. The isotopic compositions of

154   carbon ($\delta^{13}C$) and nitrogen ($\delta^{15}N$) are expressed by following equation:

155    $\delta X = (R_{sample} / R_{standard} - 1.0) \times 1000,$ (1)

156   where X, R_{sample}, and $R_{standard}$ are the target elements (C or N), and the heavy (^{13}C and ^{15}N) to

157   light (^{12}C and ^{14}N) isotope ratios of the sample and standard, respectively. The standards

158   included atmospheric N_2 for nitrogen and Vienna Pee Dee Belemnite for carbon. The precision

8

159   of the analysis varied with the amounts of carbon and nitrogen and between the spectrometers,

160   but the values were within 0.2‰ for δ^{13}C and 1‰ for δ^{15}N. Considering the quality of the

161   standards, the δ^{13}C and δ^{15}N values of each sample were rounded off to one decimal place.

162   The δ^{13}C and δ^{15}N values of the POM were sometimes the outlier values. Therefore, the

163   mean and standard deviations (sd) were calculated for δ^{13}C and δ^{15}N values for all the samples,

164   and the samples whose δ^{13}C or δ^{15}N values differed by $>3 \times$ sd from the mean values were

165   eliminated. This quality control process was performed twice. In addition, the samples for

166   which the δ^{13}C and δ^{15}N values were available, but the environmental parameters were not

167   recorded were removed. As a result, 490 samples out of 526 samples were used in the following

168   statistical analyses. The breakdown of seasonality was as follows: the numbers in winter, spring,

169   summer, and autumn were 108, 147, 133, and 102, respectively. Our data was in the

170   supplemental information.

171

172   2.3. Statistical Analysis

173   Statistical analysis was conducted using R version 4.0 [*R Core Team*, 2020]. Generalized

174   linear models (GLMs) were applied to assess the variables that predicted the δ^{13}C and δ^{15}N

175   values for seasonal and yearly variations. GLM is one of the empirical models for understanding

176   the relationships between explanatory variables and response variables. The models are

177   described as follows:

178      $\delta X \sim N(\mu, \sigma^2)$ (2)

179      $\delta X \sim \text{glm}[f(Y) + f(A):f(Sea) + f(A) + f(Sea) + T + Sal + \log\text{-Chl} + \log\text{-Nit} + Dep + K]$ (3)

180      $\delta X_{10m} \sim \text{glm}[f(Y) + f(A):f(Sea) + f(A) + f(Sea) + T + Sal + \log\text{-Chl} + \log\text{-Nit} + \log\text{-Diat} + K]$ (4)

181   where N, μ and σ^2 are the normal distribution, mean, and variance, respectively. δX correspond

182   to $\delta^{13}C$ or $\delta^{15}N$, and δX_{10m} refers to the values at a depth of 10 m, at which the phytoplankton

183   community structures are observed. Y, A, Sea, T, Sal, log-Chl, log-Nit, Dep, log-Diat, and K

184   indicate the sampling year, area (coastal or offshore), season (winter, spring, summer, or

185   autumn), temperature, salinity, common-logarithm transformed chlorophyll a concentration

186   (abbreviated as log-chlorophyll, except in the equations), common-logarithm transformed nitrate

187   concentration (log-nitrate, except in the equations), sampling depth, common-logarithm

188   transformed carbon amounts of diatoms (log-diatom, except in the equations), and latitude of the

189   Kuroshio axis, respectively. The letter "f" indicates a categorical variable. For the interaction

190   term between the area and seasons, f(A):f(Sea), it was assumed that the intercept of $\delta^{13}C$ or $\delta^{15}N$

191   is different between the areas. In these analyses, it was assumed that the environmental

192   parameters were linearly correlated to $\delta^{13}C$ or $\delta^{15}N$; hereafter, the model is described as the

193   linear function GLM. The models using the full data (eq. 3) were considered to be more reliable

194   rather than those limited by the 10 m depth (eq. 4), because the latter had only a small number of

195   data sets, which generated bias in the annual and seasonal sampling. Considering the nonlinear

196   relationship between the explanatory variables and $\delta^{13}C$ or $\delta^{15}N$, the following GLMs were also

197   applied to $\delta^{13}C$ or $\delta^{15}N$:

198     $\delta X \sim \text{glm}[f(Y) + f(A){:}f(Sea) + f(A) + f(Sea) + p(T, 4) + p(Sal, 4) + p(\text{log-Chl}), 4) + p(\text{log-Nit}, 4)$

199     $+ p(Dep, 4) + p(K, 4)]$ (5)

200   Here, $p(Z, 4)$ denotes the numerical explanatory variables (Z) applied as quartic functions

201   (degree of 4). Quartic function was selected to avoid overfitting. Hereafter, the model described

202   by eq. 5 is named as the quartic function GLM.

203   The generalized variance inflation factor (GVIF) was calculated using the "car" package

204   [*Fox and Weisberg*, 2018], and the highest GVIF parameters adjusted using the degree of

205   freedom were <10. The explanatory variables and final model descriptions were selected on the

206   basis of the Akaike Information Criterion (AIC). The "emmeans" package [*Lenth*, 2020] was

207   used to calculate the least squares mean (lsmean) values and standard errors of the yearly

208   variations based on the AIC-selected GLMs. The effects of the parameters were visualized using

209   "response.plot2" function in the "biomod2" package [*Thuiller et al.*, 2020].

210

211   **3. Results**

212   **3.1. Seasonality of environmental parameters**

213   The water temperature was the highest in summer but some cold water (<18 °C) was

214   observed in the coastal area at the subsurface [*Figure 2*]. In summer and autumn, less-saline

215   water (<34) was also found in the area [*Figure 2*], which was attributed to the warm coastal

216   water input (>22 °C). Contrary to the coastal areas, warm and high-salinity water was found in

217   the offshore areas. In the offshore area, water was less-saline in summer than that in winter and

218   spring [*Figure 2*]. The chlorophyll *a* concentration in the coastal area increased in the spring,

219   and decreased in summer [*Figure 2*]. In the offshore area, chlorophyll *a* concentrations in the

220   winter and spring were identical. Nitrate concentration was negligible near the surface from

221   spring to autumn in the offshore area and during summer in the coastal area [*Figure 2*]. At the

222   base of the eutrophic layer (1% light depth), the nitrate was not depleted even in summer. The

223   diatom abundance at a depth of 10 m was the highest during the spring in the coastal area, and it

224   was higher than that of the offshore area during all seasons [*Figure 2*]. In the offshore area, the

225   diatom abundance was identical in winter and spring, but decreased in summer and autumn.

226

3.2. Isotope ratios

228   The $\delta^{13}C$ and $\delta^{15}N$ values of POM varied between -28.7 and -20.3‰ for $\delta^{13}C$ and

229   between -4.0 and 8.0‰ for $\delta^{15}N$ ($n = 490$) [*Figure 3*]. When the data was divided into the area

230   and season, the seasonal variations of both $\delta^{13}C$ and $\delta^{15}N$ values were significant for both the

231   coastal and offshore areas (ANOVA, $p < 0.01$). The 95% probability ellipses showed that both

232   the $\delta^{13}C$ and $\delta^{15}N$ values varied most widely during spring in the coastal area, and those in

233   summer and autumn were within the variations observed during spring [*Figure 3*]. During

234   winter in the coastal area, $\delta^{13}C$ was within the range observed in the spring, but $\delta^{15}N$ was slightly

235   lower. In the offshore area, both $\delta^{13}C$ and $\delta^{15}N$ values varied most widely in the summer, and

236   those during autumn were within the ranges observed in summer. The $\delta^{13}C$ and $\delta^{15}N$ values in

237   winter and spring were slightly lower and higher, respectively, in comparison to those during

238   summer.

239

3.3. Relationship between environmental parameters and isotope ratios

241   Significant (*F*-test, $p<0.05$) linear relationships between $\delta^{13}C$ and several environmental

242   factors, *i.e.* temperature, salinity, and log-nitrate were observed [*Figure 4*]. The coefficients and

243   intercept of the linear regression between $\delta^{13}C$ and temperature were 0.060 ± 0.013 (‰°C^{-1}) and

244   -25.3 ± 0.3‰, respectively, and those between $\delta^{13}C$ and salinity were -2.1 ± 0.20 (‰) and $48.7 \pm$

245   6.6‰, respectively. The coefficient of determination (r^2) shows salinity was the strongest

246   explanatory parameter ($r^2 = 0.197$), and temperature and log-nitrate were weak parameters ($r^2 =$

247   0.037 and 0.026, respectively). There was no significant relationship between $\delta^{13}C$ and log-

248 chlorophyll ($p > 0.2$), and the latitude of the Kuroshio axis [*Figure 4*]. There was a positive

249 relationship between $\delta^{13}C$ and log-diatom [*Figure 4*].

250 Significant (*F*-test, $p < 0.05$) linear relationships were observed between $\delta^{15}N$ and both

251 salinity and log-nitrate [*Figure 5*], but both relationships were weak based on the coefficients of

252 determination ($r^2 = 0.008$ and 0.02 for salinity and log-nitrate, respectively). Significant linear

253 relationships were not observed between $\delta^{15}N$ and other environmental factors such as

254 temperature, log-chlorophyll, latitude of Kuroshio axis, and log-diatom. The $\delta^{15}N$ value of the

255 POM increased with an increase in the temperature below 20 °C, but in warm water, the linear

256 trend was not significant [*Figure 5*].

257

258 **3.4. Results of GLMs**

259 The descriptions of the least-AIC GLMs are included in *Table 1*. The sampling depth

260 was selected neither for $\delta^{13}C$ nor $\delta^{15}N$ in all the models. The selected parameters were different

261 in each model, and for $\delta^{15}N$ of the full data model with linear function, only temperature was

262 selected as the environmental parameter. Seasonal and spatial differences including their

263 interaction term were selected in the linear function models, while their interaction term was not

264 included in the quartic function models. The coefficient of determination of the GLMs using the

265 quartic function was higher than those using the linear functions. Yearly variation was not

266 selected only in the model of $\delta^{13}C$ at 10-m depth.

267 The responses of the numerical explanatory variables in the least-AIC GLMs are shown

268 in *Figure 6.* In the full data set model using only the linear functions for $\delta^{13}C$, the negative

269 effects to $\delta^{13}C$ were observed for temperature, salinity, log-nitrate, and latitude of the Kuroshio

270   axis, while the positive effect was observed for log-chlorophyll [*Figure 6*]. These relationships

271   were statistically significant, except for log-nitrate ($p < 0.05$). In the full data set model

272   considering the nonlinear effects for $\delta^{13}C$, the effect of the latitude of the Kuroshio axis was

273   different from that with the linear function: $\delta^{13}C$ showed higher values when the large mender

274   occurred [*Figure 6*]. The responses of the other parameters were not considerably different from

275   those of the linear functions [*Figure 6*]. The GLM for $\delta^{13}C$ at 10 m depth showed that log-

276   diatom significantly and positively affected the $\delta^{13}C$ values [*Figure 6*].

277   For $\delta^{15}N$, only temperature was selected and found to positively affect $\delta^{15}N$ in the GLM

278   employing linear functions, while temperature, salinity, log-chlorophyll, and log-nitrate were

279   selected in the GLM including the quartic functions [*Figure 7*]. The temperature showed a

280   unimodal distribution, and the peak of the response was observed at ~20 °C [*Figure 7*]. The

281   unimodal distribution was also observed for log-nitrate; the $\delta^{15}N$ value decreased when the

282   nitrate concentration was greater than the sub-micromolar levels [*Figure 7*]. The increases in

283   log-chlorophyll and salinity showed negative effects on $\delta^{15}N$ [*Figure 7*]. Log-diatom was

284   selected and showed negative effects on $\delta^{15}N$ [*Figure 7*], but the coefficient was not significantly

285   different from 0.

286   After considering the environmental parameters, spatial, yearly, and seasonal differences

287   were still significant, except the spatial difference of $\delta^{13}C$ estimated from the quartic function-

288   GLM [*Table 1*]. After calculating the yearly lsmean $\delta^{13}C$ and $\delta^{15}N$ values, the reduced sampling

289   frequency after 2017 resulted in large standard errors in $\delta^{13}C$ and $\delta^{15}N$, which made the yearly

290   lsmean values unreliable [*Figure 8*]. In addition, the effects of the Kuroshio large mender after

291   2018 [*Figure 1*] also made the lsmean $\delta^{13}C$ unreliable, in particular, for the values based on the

292   quartic function GLM [*Figure 8*]. Except these unreliable yearly values (*i.e.* after 2017), lsmean

14

293 ($\pm$ SE) δ^{13}C values ranged between -25.2 $\pm$ 0.1‰ (2013) and -23.4 $\pm$ 0.2‰ (2008) for the linear

294 function GLM, and between -24.9 $\pm$ 0.2‰ (2013) and -23.6 $\pm$ 0.2‰ (2008) for the quartic

295 function GLM. In contrast to δ^{13}C, δ^{15}N varied between 0.6 $\pm$ 0.2‰ (2013) and 3.1 $\pm$ 0.2‰

296 (2014) for the linear function GLM, and between 2.0 $\pm$ 0.3‰ (2013) 4.2 $\pm$ 0.3‰ (2014) for the

297 quartic function GLM. In 2013, both the lsmean values of δ^{13}C and δ^{15}N were the lowest. The

298 δ^{13}C and δ^{15}N values had no significant linear relationships to the year when the data after 2017

299 were removed.

300 For the calculation of the seasonal and spatial lsmean values, the environmental

301 parameters except season and area were fixed. However, in the observations, the environmental

302 parameters showed some degrees of collinearity to the season and/or areas. Therefore, the

303 seasonal and spatial "climatological" δ^{13}C and δ^{15}N values were calculated using the least-AIC

304 GLMs and median values of the environmental parameters of each season and area. The year

305 was fixed as 2012, when both the lsmean δ^{13}C and δ^{15}N values were neither maximum nor

306 minimum. As a result, significant spatial difference in the seasonality of δ^{13}C and δ^{15}N was

307 detected regardless of the linear and quartic function GLMs [*Figure 9*]. Because the coefficients

308 of determination (r^2 values) were greater for the quartic function GLM than those for the linear

309 function GLM [*Table 1*], the numerical values hereafter correspond to the results of the quartic

310 function GLM. In the coastal area, both the climatological δ^{13}C and δ^{15}N values were the lowest

311 in winter (-23.9 $\pm$ 0.2‰ [mean $\pm$ SE] and 0.8 $\pm$ 0.4‰, respectively). The δ^{15}N values were

312 higher than 2.5‰ and similar in the other three seasons (2.7 $\pm$ 0.4, 2.7 $\pm$ 0.4 and 3.2 $\pm$ 0.4‰ in

313 spring, summer, and autumn, respectively). The δ^{13}C values were highest in summer (-22.4 $\pm$

314 0.2‰), and those during spring and autumn were similar (-23.1 $\pm$ 0.2 and -23.2 $\pm$ 0.2,

315 respectively). In the offshore area, the seasonal δ^{13}C and δ^{15}N values varied in a narrower range

15

316   than those in the coastal area. The δ^{13}C values were lowest in winter (-24.3 ± 0.2‰) and highest

317   in summer (-22.9 ± 0.2‰), corresponding to the same trend observed in the coastal area.

318   However, the δ^{15}N value was the highest in spring (2.6 ± 0.4‰) and lowest in summer (0.9 ±

319   0.4‰). Moreover, the δ^{15}N value in the offshore area during winter (1.6 ± 0.4‰) was higher

320   than that in the coastal area.

321

4. Discussion

4.1. Comparison of the previous studies

324   In the upstream of the Kuroshio and the East China Sea, the horizontal gradients of δ^{13}C

325   and δ^{15}N of the POM were reported [*Wu et al.*, 2003] to range from -19 to -31‰ for δ^{13}C and

326   from 0.7 to 9.5‰ for δ^{15}N in autumn. *Saino and Hattori* [1987] reported only the δ^{15}N value in

327   the Philippine Sea (western North Pacific Subtropical Gyre), i.e., -1.1‰ at the surface, and

328   *Minagawa et al.* [2001] reported values between -21.6 and -24.4‰ for δ^{13}C and between ~1‰

329   and ~4‰ for δ^{15}N in the East China Sea during summer. *Takai et al.* [2007] reported the δ^{13}C

330   and δ^{15}N values of the POM ranging from -24.2 to -19.1 and 0.7 to 6.8, respectively, around the

331   Izu Peninsula, corresponding to the coastal area of our study but including the ashore area. *Mino*

332   *et al.* [2020] also reported the seasonal variations in the northern edge of the western North

333   Pacific Subtropical Gyre. In their observations, the δ^{15}N values of the POM ranged between 1.5

334   and 2.6‰ at 0–100 m depth [*Mino et al.*, 2020], but *Mino et al.* [2020] did not report the δ^{13}C

335   values. The ranges for these values are consistent with the results presented herein. Therefore,

336   considering that results in the present study are based on the over-decadal seasonal repeated

337   observations, the climatological δ^{15}N and δ^{13}C values herein [*Figure 9*] can be treated as the

16

338   seasonal climatological values in the Kuroshio area, the western boundary current of the North

339   Pacific.

340   The yearly variations in this study did not show any significant long-term trends for both

341   δ^{13}C and δ^{15}N [*Figure 8*]. This was different from the previous studies that inferred the values

342   from the δ^{13}C content of the fish muscles [*Lorrain et al.*, 2020], which suggested that the δ^{13}C

343   content of the POM decreased linearly in the 21st century. The study period in the present

344   investigation is shorter than the previous studies [*Lorrain et al.*, 2020], and decadal variations of

345   biogeochemical processes are pointed in the Kuroshio [*Oka et al.*, 2019; *Watanabe et al.*, 2005].

346   Therefore, further long-term monitoring of δ^{13}C and δ^{15}N is necessary for understanding their

347   variation trends in the POM, and for determining the anthropogenic effects of carbon and

348   nitrogen dynamics in the Kuroshio.

349

350   **4.2.   Carbon dynamics in the vicinity of the Kuroshio**

351   Both δ^{13}C and δ^{15}N values of the POM are different from those of the phytoplankton

352   because POM contains heterotrophic small planktons and detritus, but it is considered that δ^{13}C

353   and δ^{15}N values of POM are largely dependent on those of the phytoplankton in open water. The

354   δ^{13}C value of the phytoplankton depends on the CO_2 concentration in water, growth rate, and cell

355   geometry of each species [*Popp et al.*, 1998]. The growth rate of the phytoplankton depends on

356   temperature, nutrient concentration, and light conditions [*Cross et al.*, 2015], and CO_2

357   concentration in water depends on the temperature, atmospheric CO_2 concentration, and

358   phytoplankton growth. As the result, the δ^{13}C value of the POM or phytoplankton becomes

17

359   higher with an increase in the temperature [*Goericke and Fry*, 1994; *Wada et al.*, 2012], and with

360   the rapid growth of the phytoplankton [*Laws et al.*, 1995].

361   However, the δ^{13}C response to temperature was weak or negligible in the present study

362   contrary to that observed in the previous studies [*Figures 4 and 6*]. The coefficient of simple

363   linear regression analysis between temperature and δ^{13}C [*Figure 4*] was 0.06 ± 0.01 (‰ °C^{-1}),

364   which was smaller than that obtained by the global data estimation (0.17 ± 0.04) [*Goericke and*

365   *Fry*, 1994] and in western North Pacific (0.25) [*Wada et al.*, 2012]. The seasonal variations

366   indicated that the δ^{13}C value of the POM was high in warm water (for example, δ^{13}C in the

367   offshore area during summer), but the other factors such as salinity and chlorophyll *a*

368   concentration more significantly affected the δ^{13}C variations in the Kuroshio. The other possible

369   mechanism for the weak or negligible temperature response was the gravitational downward flux

370   of the POM from the warm surface water to cold subsurface water. When the downward flux

371   was active and heterogenous both in time and space, the relationship between δ^{13}C and *in situ*

372   temperature was weaker than the empirical values, because the high δ^{13}C of the POM produced

373   in the warm surface layer was mixed with the low δ^{13}C of POM produced in the cold subsurface

374   layer.

375   The highest δ^{13}C value was observed during spring in the coastal area, with a high diatom

376   carbon abundance. The carbon isotopic fractionation of the diatoms is larger than that of the

377   cyanobacteria [*Popp et al.*, 1998]. Therefore, it was considered that rapid growth of diatoms in

378   the blooms afforded the highest δ^{13}C in the POM during spring in the coastal area. In the coastal

379   area of the Kuroshio, nutrient supply during winter was significantly higher than that in the

380   offshore area [*Kodama et al.*, 2014b]. Thus, the more diatom blooms were observed compared

381   to those in the offshore area, and the δ^{13}C value of the POM in the coastal area was higher than

382   that in the offshore. The positive coefficient of log-chlorophyll for δ^{13}C in the GLM also

383   supported that δ^{13}C of POM elevates during the rapid phytoplankton growth. These observations

384   suggested that carbon sequestration during spring in the coastal area was active, and δ^{13}C of

385   POM varied with the phytoplankton community structure in the real ocean.

386   The salinity decreased during summer and autumn in the coastal area and showed a

387   negative effect on δ^{13}C [*Figures 4 and 6*]. Thus, a high δ^{13}C was observed in less-saline water

388   supply. In the estuary, the δ^{13}C value of the POM is sometimes affected by the riverine POM

389   [*Bănaru et al.*, 2014]. The intercept of the simple linear relationship between salinity and δ^{13}C

390   indicated that the δ^{13}C value of the POM in original freshwater was 48.7 ± 6.6‰ if the

391   relationship between salinity and δ^{13}C was established only based on the results of mixing

392   riverine and oceanic POM. This estimated value was unrealistic: the δ^{13}C of the riverine POM

393   was between -29.1‰ and -28.7‰ [*Nagao et al.*, 2013; *Nagao et al.*, 2010], between -12‰ and -

394   28‰ at the Ise bay, which was near the observation area of the present study [*Sugimoto et al.*,

395   2004], and -26.9 ± 1.1‰ in the Tokyo bay [*Ogawa and Ogura*, 1997]. Therefore, the high δ^{13}C

396   of the POM in the summer was not the result of the horizontal advective transport of the riverine

397   POM.

398   In addition to the POM, inorganic nutrients are also supplied by the riverine freshwater.

399   With these nutrients, the high δ^{13}C values of the POM in the estuary reported by the previous

400   studies [*Ogawa and Ogura*, 1997; *Sugimoto et al.*, 2004] are due to the phytoplankton blooms

401   (rapid growth) in the low-salinity nutrient-rich water. With low-salinity water, such a high-δ^{13}C

402   POM is possibly advected from the estuary or eutrophic ashore areas to the investigated area in

403   the present study. In fact, a high δ^{13}C was observed in the ashore area near this investigated area

404   by *Takai et al.* [2007]. Therefore, considering the $\delta^{13}C$ values, the contribution of the riverine

405   inorganic nutrients may be significant to the productivity in the coastal area of the Kuroshio.

406   The Kuroshio path also affected to $\delta^{13}C$ value of the POM in the GLMs [*Figure 6*]. The

407   coefficients of the linear function GLM suggested that when the Kuroshio flowed near the coast,

408   the $\delta^{13}C$ value of the POM decreased, and when the Kuroshio large meander occurred, the $\delta^{13}C$

409   value of the POM increased. The quartic function GLM indicated that the $\delta^{13}C$ value of the

410   POM was significantly higher when the Kuroshio large meander occurred, but considering the

411   yearly lsmean, the response to the Kuroshio path in the quartic function GLM was unreliable and

412   overfitted. Additional studies are necessary to understand the relationship between the Kuroshio

413   path and $\delta^{13}C$.

414

4.3. Nitrogen dynamics in the vicinity of the Kuroshio

416   The $\delta^{15}N$ value of the POM varies with $\delta^{15}N$ of the original nitrogen sources (nitrate,

417   ammonium, and N_2 fixation), and degree of isotopic fractionation. The rate of isotopic

418   fractionation of the phytoplankton is controlled by its growth rate [*Wada and Hattori*, 1990].

419   The highest $\delta^{15}N$ value of the POM is produced under nitrate-depleted condition, in which the

420   nitrogen isotopic fractionation of nitrate does not occur [*Wada et al.*, 2012]. The lowest $\delta^{15}N$

421   value of the phytoplankton originates from nitrogen fixation [*Minagawa and Wada*, 1986]. The

422     $\delta^{15}N$ value of the nitrate is 3–5‰ in the vicinity of the Kuroshio [*Sugimoto et al.*, 2009;

423   *Yoshikawa et al.*, 2018]. In winter, vertical mixing occurs, and nitrate is present at a micromolar

424   level both in the coastal and offshore areas in the euphotic layer [*Figure 2*]. In spring,

425   stratification starts occurring, and the nitrate in the offshore depletes but is detectable at the sub-

426   micromolar level [*Figure 2*]. The δ^{15}N value of the POM (phytoplankton) is lower than that of

427   the nitrate under conditions with sufficient nitrate [*Fogel and Cifuentes*, 1993; *Montoya and*

428   *McCarthy*, 1995; *Wada*, 1980]. Therefore, the lower climatological δ^{15}N values of the POM in

429   winter (0.8 ± 0.4 and 1.6 ± 0.4‰ in the coastal and offshore areas, respectively, Figure 9)

430   compared to those during spring were owing to the difference in the nitrate, *i.e.*, nitrate

431   consumption was lower than nitrate supply in the winter, while nitrate consumption was greater

432   than nitrate supply in the spring. Similar phenomenon was reported by *Mino et al.* [2020]. The

433   δ^{15}N value of the POM in the sediment traps [*Mino et al.*, 2020] was higher than the values in

434   water, but a decrease in the δ^{15}N value of the POM in the winter was similar because of the

435   active nitrate supply due to deep mixing.

436   During summer, nitrate was largely depleted both in the coastal and offshore areas at the

437   surface, but still remained at the base of the euphotic layer in the coastal area [*Figure 2*]. In

438   addition, ammonium was depleted in the offshore area, while it remained in the coastal area at

439   the nanomolar level [*Kodama et al.*, 2014a], and nitracline was shallower in the coastal area than

440   in the offshore area [*Kodama et al.*, 2014b]. These observations suggested that the nitrate-

441   originating new production was active in the coastal waters, but not in the offshore water.

442   Two possible sources that decrease δ^{15}N of the POM in the offshore area during summer

443   are 1) nitrogen fixation and 2) wet and dry deposition of the nitrogenous nutrients from the

444   atmosphere. First, the Kuroshio and western North Pacific are two of the "hotspots" of nitrogen

445   fixation during summer [*Shiozaki et al.*, 2010; *Shiozaki et al.*, 2018; *Shiozaki et al.*, 2015]. In the

446   microscopic observations at 10 m depth, *Trichodesmium* is not abundant but an important

447   dinitrogen-fixation phytoplankton in the Kuroshio [*Shiozaki et al.*, 2018; *Shiozaki et al.*, 2015],

448   which floats upward and accumulates at the surface [*Walsby*, 1992]. The δ^{15}N of *Trichodesmium*

449   ranges between -2.1 and 0.8‰ [*Minagawa and Wada*, 1986]. Therefore, the decrease in $\delta^{15}N$ of

450   the POM during the winter was attributed to active nitrogen fixation.

451   Second, the wet and dry deposition of nitrogenous nutrient inputs from nitrogen fixation

452   and nitrate supply from deep water in the upstream of the Kuroshio are similar during summer

453   [*Kodama et al.*, 2011], and $\delta^{15}N$ of the nitrate in rainwater is <0‰ in Japan [*Wu et al.*, 2008].

454   Therefore, the wet and dry deposition of nitrogenous nutrient inputs also decrease the $\delta^{15}N$ of the

455   POM. Both factors decreased the $\delta^{15}N$ of the POM in the offshore area during summer. In the

456   autumn, the mixing layer deepened, and the nitrate concentration again increased in the euphotic

457   layer [*Figure 2*], and thus, $\delta^{15}N$ value of the POM was a mixture of the summer values and

458   nitrate-originating values.

459   In the coastal area, the climatological $\delta^{15}N$ value in the summer was similar to that during

460   spring, suggesting that the contributions of nitrogen fixation and atmospheric deposition were

461   small during the summer. In contrast, salinity decreased in the summer; therefore, riverine

462   inputs as well as nitrogen fixation and atmospheric depositions must be considered because

463   riverine inputs of the nitrogenous nutrients possibly comprise ~10% of the nitrogenous nutrient

464   input in the coastal area [*Kodama et al.*, 2014b]. The aforementioned relationship between

465   salinity and $\delta^{13}C$ also indicated that riverine inputs of the nitrogenous nutrients influenced the

466   productivity in the coastal area. However, the $\delta^{15}N$ value of riverine nitrate varied from 0 to 8‰,

467   and decreased with an increase in the river discharge and was unstable [*Sugimoto et al.*, 2011].

468   The $\delta^{15}N$ of ammonium was high (typically >10‰), but the concentration of ammonium was

469   approximately one-third of nitrate in the river discharge [*Sugimoto et al.*, 2011]. Therefore, the

470   impact of riverine water on the $\delta^{15}N$ value of the POM was not evaluated in this study.

471   As nitrogen fixation and atmospheric deposition decreased the δ^{15}N value of the POM in

472   the offshore area, the contributions of these nitrogenous inputs were estimated. Assuming that

473   all δ^{15}N in the POM originating from nitrogen fixation, atmospheric deposition, and ammonium

474   was -1‰ [*Knapp et al.*, 2011; *Minagawa and Wada*, 1986; *Wu et al.*, 2008] and that from deep-

475   sea nitrate was 4‰ based on δ^{15}N of the nitrate [*Mino et al.*, 2020; *Sugimoto et al.*, 2009;

476   *Yoshikawa et al.*, 2018], the deep-sea nitrate-originating POM comprised only one-third of the

477   average POM (36%) in the offshore area during summer (δ^{15}N is 0.8‰). This estimated

478   contribution of the deep-sea nitrate-originating POM was possibly an overestimation because the

479   contributions of the dissolved organic nitrogen (DON), whose δ^{15}N was high, as well as that of

480   nitrate, were ignored [*Knapp et al.*, 2011]. In other seasons, nitrate concentration was often

481   detectable; thus, the isotopic fraction during nitrate assimilation was not ignored, and the

482   contribution of deep-sea nitrate must be underestimated in our calculations.

483   The source of new nitrogen is more appropriately estimated based on the δ^{15}N value of

484   the sinking POM [*Casciotti et al.*, 2008]. At station ALOHA set off Hawaii, the annual mean

485   contribution of nitrogen fixation is 26–69% of the exported POM [*Böttjer et al.*, 2017; *Casciotti*

486   *et al.*, 2008; *Dore et al.*, 2002]. At station S1 set in the western North Pacific, the annual

487   contribution of nitrogen fixation is 7–14% [*Mino et al.*, 2020]. The δ^{15}N of the POM in the

488   present study during summer was similar to that measured in the euphotic layer at station

489   ALOHA during summer [*Casciotti et al.*, 2008], slightly lower than that at station S1 [*Mino et*

490   *al.*, 2020], and higher than that in the western South Pacific Subtropical Gyre [*Shiozaki et al.*,

491   2014]. Therefore, the contributions of nitrogen fixation and atmospheric deposition to the new

492   production in the Kuroshio area during summer and at station ALOHA are significant, but these

493   are not lower than those in the western South Pacific Subtropical Gyre, and are at least one-

494 quarter of the new production in this area. Considering the yearly lsmean of δ^{15}N, the

495 contribution of deep-sea nitrate varies interannually. For example, its contribution was ~30%

496 lower than the average in 2013 in both the models, but the reason was not clear in this study.

497

498 **5. Conclusion**

499   This study reports the seasonal variations in the δ^{13}C and δ^{15}N values of the POM in the

500 euphotic layer based on the middle term (~10 years) repeated seasonal observations. The spatio-

501 seasonal variations in δ^{13}C and δ^{15}N of POM show that the primary production in the vicinity of

502 the Kuroshio is supported by many physical and biological processes, i.e., during the nitrate-

503 sufficient and well-mixed conditions in winter, a low δ^{15}N indicates the dominance of nitrate-

504 originating primary production. When the stratification develops, and nitrate depletes in the

505 spring, a high δ^{15}N suggests that the isotopic fractionation of nitrate does not occur. In the

506 summer, diazotrophs and atmospheric deposition play important roles in the primary production

507 in the offshore area, while contribution from deep-sea nitrate remains active in the coastal area;

508 the contribution of riverine nitrogenous nutrient is considered significant, but cannot be

509 evaluated based on δ^{15}N. The deep-sea nitrate-originating production is considered to be limited

510 to one-third of primary production in the offshore area during summer. The carbon dynamics

511 also exhibit spatio-seasonality. In the coastal area, the spring diatom blooms result in high δ^{13}C-

512 POM, whereas in the offshore, high δ^{13}C-POM is formed in the summer. High δ^{13}C-POM is also

513 present in low-salinity water in the coastal area, which may be caused by the horizontal

514 advection of the ashore water, and significantly affects the primary production in the coastal

515 area. Therefore, complex biogeochemical processes support the primary production in the

516 vicinity of the Kuroshio and the subsequent fishery production in the Pacific.

517   The yearly variation of the lsmean δ^{15}N indicates that the proportion of deep-sea nitrate

518   and nitrogen fixation or atmospheric deposition for the new production is not homogenous.

519   However, the yearly linear trends and the effect of the Kuroshio large mender are not clearly

520   observed because the Kuroshio large mender occurred after 2018; recent changes in the δ^{15}N and

521   δ^{13}C values of the POM are not sufficient to elucidate the effects. As the Kuroshio path shows a

522   large impact on the ecosystems in the Kuroshio [*Hiraoka et al.*, 2019; *Nakata et al.*, 2000],

523   further studies are necessary to understand the yearly variations and anthropogenic impact on the

524   primary production of the Kuroshio area.

525

Acknowledgement

537   **Table 1**. Descriptions of the least Akaike Information Criterion generalized linear models (AIC GLMs)

538   and their coefficients of determination (r^2). The abbreviations are the same as those described in eq. 3.

Least AIC models	r^2
Linear function	
$\delta^{13}C$ f(Y) + f(A):f(Sea) + f(A) + f(Sea) + T + Sal + log-chl + log-nit + K	0.443
$\delta^{15}N$ f(Y) + f(A):f(Sea) + T	0.309
Quartic function	
$\delta^{13}C$ f(Y) + f(Sea) + p(T) + p(Sal) + p(log-chl) + p(log-nit) + p(K)	0.596
$\delta^{15}N$ f(Y) + f(A) + f(Sea) + p(T) + p(Sal) + p(log-chl) + p(log-nit)	0.387
Linear function including diatom abundance (10 m depth only)	
$\delta^{13}C_{10\,m}$ f(A) + f(Sea) + Sal + log-Chl + log-Nit + log-Diat + K	0.817
$\delta^{15}N_{10\,m}$ f(Y) + f(A):f(Sea) + f(A) + f(Sea) + T + log-Chl + log-Nit + log-Diat	0.659

539

540   **References**

541   Aita, M. N., K. Tadokoro, N. O. Ogawa, F. Hyodo, R. Ishii, S. L. Smith, T. Saino, M. J. Kishi, S.-I.
542   Saitoh, and E. Wada (2011), Linear relationship between carbon and nitrogen isotope ratios along
543   simple food chains in marine environments, *J. Plankton Res.*, *33*(11), 1629-1642,
544   doi:10.1093/plankt/fbr070.

545   Archer, D., et al. (2009), Atmospheric lifetime of fossil fuel carbon dioxide, *Annu. Rev. Earth Planet. Sci.*,
546   *37*(1), 117-134, doi:10.1146/annurev.earth.031208.100206.

547   Bănaru, D., F. Carlotti, A. Barani, G. Grégori, N. Neffati, and M. Harmelin-Vivien (2014), Seasonal
548   variation of stable isotope ratios of size-fractionated zooplankton in the Bay of Marseille (NW
549   Mediterranean Sea), *J. Plankton Res.*, *36*(1), 145-156, doi:10.1093/plankt/fbt083.

550   Böttjer, D., J. E. Dore, D. M. Karl, R. M. Letelier, C. Mahaffey, S. T. Wilson, J. Zehr, and M. J. Church
551   (2017), Temporal variability of nitrogen fixation and particulate nitrogen export at Station
552   ALOHA, *Limnol. Oceanogr.*, *62*(1), 200-216, doi:10.1002/lno.10386.

553   Casciotti, K. L., T. W. Trull, D. M. Glover, and D. Davies (2008), Constraints on nitrogen cycling at the
554   subtropical North Pacific Station ALOHA from isotopic measurements of nitrate and particulate
555   nitrogen, *Deep Sea Res. II*, *55*(14), 1661-1672, doi:10.1016/j.dsr2.2008.04.017.

556   Chiba, S., H. Sugisaki, A. Kuwata, K. Tadokoro, T. Kobari, A. Yamaguchi, and D. L. Mackas (2012), Pan-
557   North Pacific comparison of long-term variation in Neocalanus copepods based on stable isotope
558   analysis, *Prog. Oceanogr.*, *97-100*, 63-75, doi:10.1016/j.pocean.2011.11.007.

559   Christensen, J. T., and K. Richardson (2008), Stable isotope evidence of long-term changes in the North
560   Sea food web structure, *Mar. Ecol. Prog. Ser.*, *368*, 1-8, doi:10.3354/meps07635.

561   Cross, W. F., J. M. Hood, J. P. Benstead, A. D. Huryn, and D. Nelson (2015), Interactions between
562   temperature and nutrients across levels of ecological organization, *Glob Chang Biol*, *21*(3), 1025-
563   1040, doi:10.1111/gcb.12809.

564   Dore, J. E., J. R. Brum, L. M. Tupas, and D. M. Karl (2002), Seasonal and interannual variability in
565   sources of nitrogen supporting export in the oligotrophic subtropical North Pacific Ocean,
566   *Limnol. Oceanogr.*, *47*(6), 1595-1607, doi:10.4319/lo.2002.47.6.1595.

567   Duce, R. A., et al. (2008), Impacts of atmospheric anthropogenic nitrogen on the open ocean, *Science*,
568   *320*(5878), 893-897, doi:10.1126/science.1150369.

569   Fogel, M. L., and L. A. Cifuentes (1993), Isotope fractionation during primary production, in *Org.*
570   *Geochem.*, edited by M. H. Engel and S. A. Macko, pp. 73-98, Springer US, Boston, MA,
571   doi:10.1007/978-1-4615-2890-6_3.

572   Fowler, D., M. Coyle, U. Skiba, M. A. Sutton, J. N. Cape, S. Reis, L. J. Sheppard, A. Jenkins, B.
573   Grizzetti, and J. N. Galloway (2013), The global nitrogen cycle in the twenty-first century, *Philos.*
574   *T. R. Soc. B*, *368*(1621), 20130164, doi:10.1098/rstb.2013.0164.

575   Fox, J., and S. Weisberg (2018), *An R companion to applied regression*, Sage publications.

576   Goericke, R., and B. Fry (1994), Variations of marine plankton δ13C with latitude, temperature, and
577   dissolved CO2 in the world ocean, *Global Biogeochem. Cycles*, *8*(1), 85-90,
578   doi:10.1029/93gb03272.

579   Gruber, N., C. D. Keeling, R. B. Bacastow, P. R. Guenther, T. J. Lueker, M. Wahlen, H. A. J. Meijer, W.
580   G. Mook, and T. F. Stocker (1999), Spatiotemporal patterns of carbon-13 in the global surface
581   oceans and the oceanic suess effect, *Global Biogeochem. Cycles*, *13*(2), 307-335,
582   doi:10.1029/1999gb900019.

583   Hiraoka, Y., K. Fujioka, H. Fukuda, M. Watai, and S. Ohshimo (2019), Interannual variation of the diet
584   shifts and their effects on the fatness and growth of age-0 Pacific bluefin tuna (*Thunnus*
585   *orientalis*) off the southwestern Pacific coast of Japan, *Fish. Oceanogr.*, *28*(4), 419-433,
586   doi:10.1111/fog.12421.

587   Horii, S., K. Takahashi, T. Shiozaki, F. Hashihama, and K. Furuya (2018), Stable isotopic evidence for the
588   differential contribution of diazotrophs to the epipelagic grazing food chain in the mid-Pacific
589   Ocean, *Global Ecol. Biogeogr.*, *27*(12), 1467-1480, doi:10.1111/geb.12823.

590   Ishii, M., N. Kosugi, D. Sasano, S. Saito, T. Midorikawa, and H. Y. Inoue (2011), Ocean acidification off
591   the south coast of Japan: A result from time series observations of CO2parameters from 1994 to
592   2008, *J. Geophys. Res.*, *116*(C6), doi:10.1029/2010jc006831.

593   Keeling, C. D. (1979), The Suess effect: 13Carbon-14Carbon interrelations, *Environ. Int.*, *2*(4-6), 229-
594   300, doi:10.1016/0160-4120(79)90005-9.

595   Knapp, A. N., D. M. Sigman, F. Lipschultz, A. B. Kustka, and D. G. Capone (2011), Interbasin isotopic
596   correspondence between upper-ocean bulk DON and subsurface nitrate and its implications for
597   marine nitrogen cycling, *Global Biogeochem. Cycles*, *25*(4), doi:10.1029/2010gb003878.

598   Kodama, T., K. Furuya, F. Hashihama, S. Takeda, and J. Kanda (2011), Occurrence of rain-origin nitrate
599   patches at the nutrient-depleted surface in the East China Sea and the Philippine Sea during
600   summer, *J. Geophys. Res.*, *116*(C8), C08003, doi:10.1029/2010jc006814.

601   Kodama, T., T. Ichikawa, K. Hidaka, and K. Furuya (2014a), A highly sensitive and large concentration
602   range colorimetric continuous flow analysis for ammonium concentration, *J. Oceanogr.*, *71*(1),
603   65-75, doi:10.1007/s10872-014-0260-6.

604   Kodama, T., T. Setou, M. Masujima, M. Okazaki, and T. Ichikawa (2015), Intrusions of excess nitrate in
605   the Kuroshio subsurface layer, *Cont. Shelf Res.*, *110*, 191-200, doi:10.1016/j.csr.2015.10.012.

606   Kodama, T., Y. Shimizu, T. Ichikawa, Y. Hiroe, A. Kusaka, H. Morita, M. Shimizu, and K. Hidaka
607   (2014b), Seasonal and spatial contrast in the surface layer nutrient content around the Kuroshio
608   along 138°E, observed between 2002 and 2013, *J. Oceanogr.*, *70*(6), 489-503,
609   doi:10.1007/s10872-014-0245-5.

610   Laws, E. A., B. N. Popp, R. R. Bidigare, M. C. Kennicutt, and S. A. Macko (1995), Dependence of
611   phytoplankton carbon isotopic composition on growth rate and [CO2)aq: Theoretical

612   considerations and experimental results, *Geochim. Cosmochim. Acta*, *59*(6), 1131-1138,
613   doi:10.1016/0016-7037(95)00030-4.

614 Lenth, R. (2020), emmeans: Estimated marginal means, aka least-squares means, edited, https://CRAN.R-
615   project.org/package=emmean.

616 Lorrain, A., et al. (2020), Trends in tuna carbon isotopes suggest global changes in pelagic phytoplankton
617   communities, *Glob Chang Biol*, *26*(2), 458-470, doi:10.1111/gcb.14858.

618 Menden-Deuer, S., and E. J. Lessard (2000), Carbon to volume relationships for dinoflagellates, diatoms,
619   and other protist plankton, *Limnol. Oceanogr.*, *45*(3), 569-579, doi:10.4319/lo.2000.45.3.0569.

620 Minagawa, M., M. Ohashi, T. Kuramoto, and N. Noda (2001), δ15N of PON and nitrate as a clue to the
621   origin and transformation of nitrogen in the subarctic North Pacific and its marginal sea, *J.*
622   *Oceanogr.*, *57*(3), 285-300, doi:10.1023/a:1012430512137.

623 Minagawa, M., and E. Wada (1986), Nitrogen isotope ratios of red tide organisms in the East China Sea:
624   A characterization of biological nitrogen fixation, *Mar. Chem.*, *19*(3), 245-259, doi:10.1016/0304-
625   4203(86)90026-5.

626 Mino, Y., et al. (2020), Seasonal and Interannual Variations in Nitrogen Availability and Particle Export in
627   the Northwestern North Pacific Subtropical Gyre, *J. Geophys. Res.*, *125*(5), e2019JC015600,
628   doi:10.1029/2019jc015600.

629 Montoya, J. P., and J. J. McCarthy (1995), Isotopic fractionation during nitrate uptake by phytoplankton
630   grown in continuous culture, *J. Plankton Res.*, *17*(3), 439-464, doi:10.1093/plankt/17.3.439.

631 Nagao, S., T. Aramaki, N. Fujitake, H. Kodama, T. Tanaka, S. Ochiai, M. Uchida, Y. Shibata, and M.
632   Yamamoto (2013), Variation of Δ14C and δ13C values of dissolved humic and fulvic acids in the
633   Tokachi river system in northern Japan, *Radiocarbon*, *55*(Nr2-3), 1007-1016.

634 Nagao, S., T. Aramaki, O. Seki, M. Uchida, and Y. Shibata (2010), Carbon isotopes and lignin
635   composition of POC in a small river in Bekanbeushi Moor, northern Japan, *Nuclear Instruments*
636   *and Methods in Physics Research Section B: Beam Interactions with Materials and Atoms*, *268*(7-
637   8), 1098-1101, doi:10.1016/j.nimb.2009.10.108.

638 Nakata, H., S. Funakoshi, and M. Nakamura (2000), Alternating dominance of postlarval sardine and
639   anchovy caught by coastal fishery in relation to the Kuroshio meander in the Enshu-nada Sea,
640   *Fish. Oceanogr.*, *9*(3), 248-258, doi:10.1046/j.1365-2419.2000.00140.x.

641 Ogawa, N., and N. Ogura (1997), Dynamics of particulate organic matter in the Tamagawa estuary and
642   inner Tokyo Bay, *Estuar. Coast. Shelf. Sci.*, *44*(3), 263-273, doi:10.1006/ecss.1996.0118.

643 Ohshimo, S., D. J. Madigan, T. Kodama, H. Tanaka, K. Komoto, S. Suyama, T. Ono, and T. Yamakawa
644   (2019), Isoscapes reveal patterns of δ13C and δ15N of pelagic forage fish and squid in the
645   Northwest Pacific Ocean, *Prog. Oceanogr.*, *175*, 124-138, doi:10.1016/j.pocean.2019.04.003.

646 Oka, E., M. Ishii, T. Nakano, T. Suga, S. Kouketsu, M. Miyamoto, H. Nakano, B. Qiu, S. Sugimoto, and
647   Y. Takatani (2018), Fifty years of the 137°E repeat hydrographic section in the western North
648   Pacific Ocean, *J. Oceanogr.*, *74*(2), 115-145, doi:10.1007/s10872-017-0461-x.

649 Oka, E., K. Yamada, D. Sasano, K. Enyo, T. Nakano, and M. Ishii (2019), Remotely forced decadal
650   physical and biogeochemical variability of North Pacific Subtropical Mode water over the last 40
651   years, *Geophys. Res. Lett.*, *46*(3), 1555-1561, doi:10.1029/2018gl081330.

652 Popp, B. N., E. A. Laws, R. R. Bidigare, J. E. Dore, K. L. Hanson, and S. G. Wakeham (1998), Effect of
653   phytoplankton cell geometry on carbon isotopic fractionation, *Geochim. Cosmochim. Acta*, *62*(1),
654   69-77, doi:10.1016/s0016-7037(97)00333-5.

655 R Core Team (2020), R: A language and environment for statistical computing, edited by R Foundation
656   for Statistical Computing, https://www.R-project.org/. Vienna, Austria.

657 Ren, H., Y. C. Chen, X. T. Wang, G. T. F. Wong, A. L. Cohen, T. M. DeCarlo, M. A. Weigand, H. S. Mii,
658   and D. M. Sigman (2017), 21st-century rise in anthropogenic nitrogen deposition on a remote
659   coral reef, *Science*, *356*(6339), 749-752, doi:10.1126/science.aal3869.

660 Saino, T., and A. Hattori (1987), Geographical variation of the water column distrubution of suspended
661   particulate organic nitrogen and its 15N natural abundance in the Pacific and its marginal seas,
662   *Deep Sea Res. A*, *34*(5-6), 807-827, doi:10.1016/0198-0149(87)90038-0.

663 Shiozaki, T., K. Furuya, T. Kodama, S. Kitajima, S. Takeda, T. Takemura, and J. Kanda (2010), New
664   estimation of N2 fixation in the western and central Pacific Ocean and its marginal seas, *Global
665   Biogeochem. Cycles*, *24*(1), GB1015, doi:10.1029/2009gb003620.

666 Shiozaki, T., T. Kodama, and K. Furuya (2014), Large-scale impact of the island mass effect through
667   nitrogen fixation in the western South Pacific Ocean, *Geophys. Res. Lett.*, *41*(8), 2907-2913,
668   doi:10.1002/2014GL059835.

669 Shiozaki, T., Y. Kondo, D. Yuasa, and S. Takeda (2018), Distribution of major diazotrophs in the surface
670   water of the Kuroshio from northeastern Taiwan to south of mainland Japan, *J. Plankton Res.*,
671   *40*(4), 407-419, doi:10.1093/plankt/fby027.

672 Shiozaki, T., S. Takeda, S. Itoh, T. Kodama, X. Liu, F. Hashihama, and K. Furuya (2015), Why is
673   Trichodesmium abundant in the Kuroshio?, *Biogeosciences*, *12*(23), 6931-6943, doi:10.5194/bg-
674   12-6931-2015.

675 Sigman, D. M., K. L. Karsh, and K. L. Casciotti (2009), Nitrogen isotopes in the ocean, in *Encyclopedia
676   of Ocean Sciences*, edited by J. H. Steele, pp. 40-54, Academic Press, Oxford, doi:10.1016/b978-
677   012374473-9.00632-9.

678 Sonnerup, R. E., P. D. Quay, A. P. McNichol, J. L. Bullister, T. A. Westby, and H. L. Anderson (1999),
679   Reconstructing the oceanic 13C Suess Effect, *Global Biogeochem. Cycles*, *13*(4), 857-872,
680   doi:10.1029/1999gb900027.

681   Sugimoto, R., A. Kasai, K. Fujita, K. Sakaguchi, and T. Mizuno (2011), Assessment of nitrogen loading
682   from the Kiso-Sansen Rivers into Ise Bay using stable isotopes, *J. Oceanogr.*, *67*(2), 231-240,
683   doi:10.1007/s10872-011-0022-7.

684   Sugimoto, R., A. Kasai, T. Miyajima, and K. Fujita (2009), Nitrogen isotope ratios of nitrate as a clue to
685   the origin of nitrogen on the Pacific coast of Japan, *Cont. Shelf Res.*, *29*(10), 1303-1309,
686   doi:10.1016/j.csr.2009.03.007.

687   Sugimoto, R., A. Kasai, S. Yamao, T. Fujiwara, and T. Kimura (2004), Variation in particulate organic
688   matter accompanying changes of river discharge in Ise Bay, *Bull. Jap. Soc. Fish. Oceanogr.*,
689   *68*(3), 142-150.

690   Takai, N., N. Hirose, T. Osawa, K. Hagiwara, T. Kojima, Y. Okazaki, T. Kuwae, T. Taniuchi, and K.
691   Yoshihara (2007), Carbon source and trophic position of pelagic fish in coastal waters of south-
692   eastern Izu Peninsula, Japan, identified by stable isotope analysis, *Fish. Sci.*, *73*(3), 593-608,
693   doi:10.1111/j.1444-2906.2007.01372.x.

694   Tanaka, Y., A. Tawa, T. Ishihara, E. Sawai, M. Nakae, M. Masujima, and T. Kodama (2019), Occurrence
695   of Pacific bluefin tuna *Thunnus orientalis* larvae off the Pacific coast of Tohoku area,
696   northeastern Japan: Possibility of the discovery of the third spawning ground, *Fish. Oceanogr.*,
697   *29*(1), 46-51, doi:10.1111/fog.12445.

698   Tawa, A., T. Kodama, K. Sakuma, T. Ishihara, and S. Ohshimo (2020), Fine-scale horizontal distributions
699   of multiple species of larval tuna off the Nansei Islands, Japan, *Mar. Ecol. Prog. Ser.*, *636*, 123-
700   137, doi:10.3354/meps13216.

701   Thuiller, W., D. Georges, R. Engler, and F. Breiner (2020), biomod2: Ensemble Platform for Species
702   Distribution Modeling, edited.

703   Volkman, J. K., and E. Tanoue (2002), Chemical and biological studies of particulate organic matter in the
704   ocean, *J. Oceanogr.*, *58*(2), 265-279, doi:10.1023/A:1015809708632.

705   Wada, E. (1980), Nitrogen isotope fractionation and its significance in biogeochemical processes
706   occurring in marine environments, in *Isotope Marine Chemistry*, edited by E. Goldberg, Y. Horibe
707   and K. Saruhashi, pp. 375-398, Uchida Rokakuho, Tokyo.

708   Wada, E., and A. Hattori (1990), *Nitrogen in the sea: forms, abundance, and rate processes*, CRC press,
709   Florida, USA.

710   Wada, E., K. Ohki, S. Yoshikawa, P. L. Parker, C. V. Baalen, G. I. Matsumoto, M. N. Aita, and T. Saino
711   (2012), Ecological aspects of carbon and nitrogen isotope ratios of cyanobacteria, *Plank. Benth.*
712   *Res.*, *7*(3), 135-145, doi:10.3800/pbr.7.135.

713   Walsby, A. E. (1992), The gas vesicles and buoyancy of *Trichodesmium*, in *Marine Pelagic*
714   *Cyanobacteria: Trichodesmium and other Diazotrophs*, edited by E. J. Carpenter, D. G. Capone
715   and J. G. Rueter, pp. 141-161, Springer Netherlands, Dordrecht, doi:10.1007/978-94-015-7977-
716   3_9.

717   Watanabe, Y. W., H. Ishida, T. Nakano, and N. Nagai (2005), Spatiotemporal decreases of nutrients and
718   chlorophyll-*a* in the surface mixed layer of the western North Pacific from 1971 to 2000, *J.*
719   *Oceanogr.*, *61*(6), 1011-1016, doi:10.1007/s10872-006-0017-y.

720   Wu, J., Y. Nishijima, and H. Satake (2008), Seasonal variation of δ15N of nitrate ion found in
721   precipitation at Toyama, *Chikyukagaku*, *42*(1), 1-11, doi:10.14934/chikyukagaku.42.1.

722   Wu, Y., J. Zhang, D. J. Li, H. Wei, and R. X. Lu (2003), Isotope variability of particulate organic matter at
723   the PN section in the East China Sea, *Biogeochemistry*, *65*(1), 31-49,
724   doi:10.1023/a:1026044324643.

725   Yoshikawa, C., A. Makabe, Y. Matsui, T. Nunoura, and N. Ohkouchi (2018), Nitrate isotope distribution
726   in the Subarctic and Subtropical North Pacific, *Geochemistry, Geophysics, Geosystems*, *19*(7),
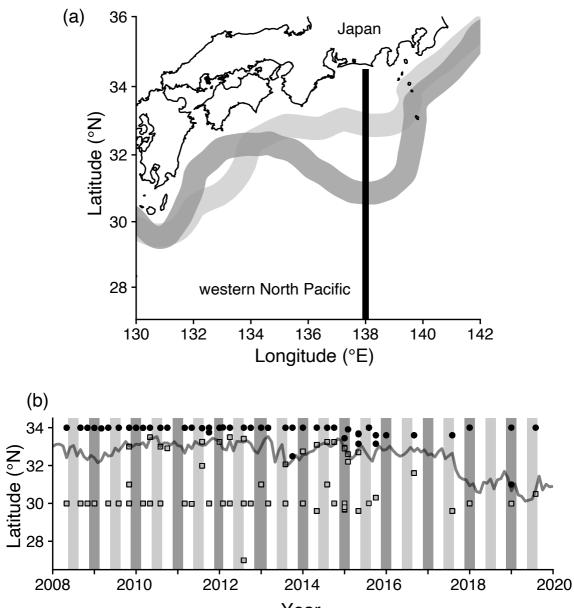727   2212-2224, doi:10.1029/2018gc007528.

728

729

731 **Figure 1**. (a) Map of the sampling site and depiction of the flow of the Kuroshio current. Light

732 and dark gray lines represent the normal path (January 2015) and large-meandered

733 path of the Kuroshio current (January 2018), respectively. Black line depicts the "O-

734 line". (b) Temporal variations of the sampling stations (circles and squares) and the

735 Kuroshio axis (solid gray line) along the O-line. Light and dark gray boxes in (b)

736 denote the summer and winter periods, respectively. Closed circles and squares

737 correspond to the coastal and offshore stations, respectively.

738 **Figure 2**. Seasonal variations in (a) temperature, (b) salinity, (c) chlorophyll a concentration, (d)

739 nitrate concentration, and (e) carbon-based diatom abundance. Dark blue and green

740 boxes indicate the data in the coastal and offshore areas, respectively. Chlorophyll *a*

741 concentration, nitrate concentration, and carbon-based diatom abundance are

742 converted into common-logarithm values. Each boxplot shows the medians (vertical

743 thick lines within boxes), upper and lower quartiles (boxes), quartile deviations

744 (horizontal bars), and outliers (circles).

745 **Figure 3**. Scatter diagrams for $\delta^{15}N$ and $\delta^{13}C$ of POM along the O-line in the (a) coastal and (b)

746 offshore areas. Circles and crosses indicate the samples collected in the coastal and

747 offshore areas, and the colors denote the different seasons. The ellipses include 95%

748 probability ellipse for each season and area.

749 **Figure 4**. Relationship between $\delta^{13}C$ and (a) temperature, (b) salinity, (c) common-logarithm

750 transformed chlorophyll a concentration (log-chlorophyll), (d) common-logarithm

751 transformed nitrate concentration (log-nitrate), (e) latitude of the Kuroshio axis, and (f)

752 common-logarithm transformed carbon-based diatom abundance (log-diatom).

34

753   Diatom abundance data is available at only 10-m depth. The colors and shapes denote

754   the areas and seasons, respectively (blue: coastal; green: offshore; closed circle:

755   winter; open triangle: spring; cross: summer; closed square: autumn). The gray solid

756   dashed line with shadow represents the linear regression line and 95% confidence

757   values. When the linear regression line is the dashed line, the linear regression

758   relationship is not significant ($p > 0.05$).

759   **Figure 5**. Relationship between $\delta^{15}N$ and (a) temperature, (b) salinity, (c) common-logarithm

760   transformed chlorophyll a concentration (log-chlorophyll), (d) common-logarithm

761   transformed nitrate concentration (log-nitrate), (e) latitude of the Kuroshio axis, and (f)

762   common-logarithm transformed carbon-based diatom abundance (log-diatom).

763   Diatom abundance data is available at only 10-m depth. The colors and shapes denote

764   the areas and seasons, respectively (blue: coastal; green: offshore; closed circle:

765   winter; open triangle: spring; cross: summer; closed square: autumn). The gray solid

766   dashed line with shadow represents the linear regression line and 95% confidence

767   values. When the linear regression line is the dashed line, the linear regression

768   relationship is not significant ($p > 0.05$).

769   **Figure 6**. Responses of the least-AIC GLMs to $\delta^{13}C$ in terms of (a) temperature, (b) salinity, (c)

770   log-chlorophyll, (d) log-nitrate, (e) latitude of the Kuroshio axis, and (f) log-diatom.

771   Solid and dotted lines denote the GLMs of $\delta^{13}C$ fitting with the linear and quartic

772   functions, respectively. Blue and green vertical ticks on the x-axes indicate the data

773   points of the coastal and offshore areas, respectively. The numerical values of

774   common-log transformed values (c, d, and f) are re-transformed to the normal values,

775   but the axes are shown with the common-log transformed values.

776 **Figure 7**. Responses of the least-AIC GLMs to δ^{15}N in terms of (a) temperature, (b) salinity, (c)

777 log-chlorophyll, (d) log-nitrate, (e) latitude of the Kuroshio axis, and (f) log-diatom.

778 Solid and dotted lines denote the GLMs of δ^{15}N fitting with the linear and quartic

779 functions, respectively. Blue and green vertical ticks on the x-axes indicate the data

780 points of the coastal and offshore areas, respectively. The numerical values of

781 common-log transformed values (c, d, and f) are re-transformed to the normal values,

782 but the axes are shown with common-log transformed values. Gray horizontal lines

783 denote that the parameter is not selected in the least-AIC GLMs.

784 **Figure 8**. Yearly variations in the least square means (lsmean, closed circle) of δ^{13}C (a, b) and

785 δ^{15}N (c, d) based on the linear GLM (a, c) and quartic GLM (b, d). Vertical lines

786 denote the 2 × standard errors (*i.e.*, 95% confidence intervals).

787 **Figure 9**. Scatter plot of the calculated climatological δ^{13}C and δ^{15}N values in each season and

788 area based on the seasonal and spatial median values. The colors denote the seasons,

789 and the shapes denote the combination of areas (open: offshore; closed: coastal) and

790 models (square: linear function GLMs; circle: quartic function GLMs).

Figure 1.

(a)

Japan

western North Pacific

(b)

Figure 2.

(a) Temperature (°C)
(b) Salinity
(c) Chlorophyll *a* (μg L⁻¹)
(d) Nitrate (μM)
(e) Ditaoms (μgC L⁻¹)

Figure 3.

Figure. (a) Coastal and (b) Offshore isotopic niche plots of $\delta^{15}N$ versus $\delta^{13}C$ by season (spring, summer, autumn, winter).

Figure 4.

(a) Temperature (°C) vs $\delta^{13}C$

(b) Salinity vs $\delta^{13}C$

(c) Log-chlorophyll [log10(μg L^{-1})] vs $\delta^{13}C$

(d) Log-nitrate [log10(μM)] vs $\delta^{13}C$

(e) Latitude of Kuroshio (°N) vs $\delta^{13}C$

(f) Log-diatom [log10(μgC L^{-1})] vs $\delta^{13}C$

Figure 5.

(a) Temperature (°C) vs δ¹⁵N

(b) Salinity vs δ¹⁵N

(c) Log-chlorophyll [log10(μg L^{-1})] vs δ¹⁵N

(d) Log-nitrate [log10(μM)] vs δ¹⁵N

(e) Latitude of Kuroshio (°N) vs δ¹⁵N

(f) Log-diatom [log10(μgC L^{-1})] vs δ¹⁵N

Figure 6.

Figure 7.

Figure 8.

Figure 9.